NASA Contractor Report 4306

# Effect of Suction on Controlling the Secondary Instability of Boundary Layers

Nabil M. El-Hady

CONTRACT NAS1-18599
JULY 1990



NASA

NASA Contractor Report 4306

# Effect of Suction on Controlling the Secondary Instability of Boundary Layers

Nabil M. El-Hady
*Analytical Services & Materials, Inc.*
*Hampton, Virginia*

Prepared for
Langley Research Center
under Contract NAS1-18599

National Aeronautics and
Space Administration
Office of Management
Scientific and Technical
Information Division

**1990**

**Page intentionally left blank**

# EFFECT OF SUCTION ON CONTROLLING THE SECONDARY INSTABILITY OF BOUNDARY LAYERS

*Nabil M. El-Hady*

Analytical Services & Materials, Inc., Hampton, Virginia 23666

*ABSTRACT*

The effect of suction on controlling the three-dimensional secondary instability is investigated for a boundary layer with pressure gradient in the presence of small but finite amplitude Tollmien-Schlichting wave. The focus is on principal parametric resonance responsible for strong growth of subharmonics in low disturbance environment. Calculations are presented for the effect of suction on the onset and amplification of the secondary instability in Blasius and Falkner-Skan flows, as well as its effect on controlling the production of the vortical structure.

May 21, 1990

# EFFECT OF SUCTION ON CONTROLLING THE SECONDARY INSTABILITY OF BOUNDARY LAYERS

*Nabil M. El-Hady*

Analytical Services & Materials, Inc., Hampton, Virginia 23666

## 1. INTRODUCTION

Laminarization of the flow by suction, and subsequent viscous drag reduction, is the principal and most effective means used for laminar flow control (LFC) [1]. Excessive suction increases suction drag and reduces the overall efficiency of an aircraft with LFC. Moreover, the over-thinned boundary layer is over-sensitive to surface irregularities. Hence, it is necessary to keep the boundary layer laminar with the least possible suction. For this purpose, the stability characteristics of the flow need to be accurately calculated, and the laminar-turbulent transition process must be well understood. Moreover, the effect of suction control on some of the early stages to transition need to be assessed.

The nonlinear process of the flow once initiated becomes violent and lead rapidly to transition, and it is then extremely difficult to control the flow field. Hence, suction control in LFC systems is preferred to be in the linear range. For these systems to be efficient, some disturbance growth should be allowed, and linear primary stability theory in conjunction with the $e^n$ method were relied on for such predictions [2]. A linear growth of a primary two-dimensional (2D) Tollmien-Schlichting (TS) wave may parametrically excite a linear secondary growth with three-dimensional (3D) character. This secondary instability may not lead to transition by itself, but as it grows, it interacts with both the mean flow and the TS wave leading rapidly to transition. The effect of suction on the primary TS wave is well established and known to be drastic [3]. While, in this paper, we are concerned with the effect of suction on controlling the onset and growth of the secondary 3D instability.

Following the growth of the primary 2D wave, the flow takes on an increasingly three-dimensional (3D) behavior [4] with explosive growth rates. In this early stage of transition, the 3D phenomenon is characterized by a strong secondary instability with respect to 3D disturbances in the presence of small but finite amplitude primary 2D waves [5,6]. Primary 3D disturbances might be stable or very slowly growing in the absence of the 2D waves. This secondary instability has been recognized experimentally (Refs. 7-12) and observed numerically (Refs. 13-18) in the uncontrolled boundary layer (Refs. 7-15) as well as the controlled boundary layer (Refs. 16-18).

Two major types of breakdown have been identified, a fundamental breakdown (K-type) and a subharmonic breakdown (H/C-type). The experiments indicate that the subharmonic breakdown occurs when the amplitude of the primary TS wave is low or moderate, while the fundamental breakdown occurs for higher amplitudes. However, one type or a mixture of both will appear depending largely on the spectrum of the background disturbances [19]. The linear secondary instability theory formulated by Herbert [20] can predict the increasingly 3D behavior with large growth rates that occur in both the fundamental and subharmonic types of breakdown, while Craik's resonant triad model [21] predicts an instability of the subharmonic type. Craik's mechanism (referred to as C-type) is thought to dominate at low amplitude of the TS wave, while Herbert's subharmonic mechanism (referred to as H-type) reflects the situation at moderate amplitudes of the TS wave. A recent review on the subject of secondary instability has been provided by Herbert [22] and Bayly et al. [23].

The 3D subharmonic instability which characterizes the road to transition initiated from a low disturbance background appears to be more realistic in flight applications. Hence, in this paper we investigate the development of the subharmonic secondary instability in a boundary layer with pressure gradients controlled by suction. Our objective is to evaluate the effect of suction control on this early stage leading to transition. Several questions need to be answered, Does suction delay the onset of the secondary instability ? How sensitive is the growth of the secondary instability to the intensity of suction ? What is the effect of the initial amplitude of

the primary wave on this sensitivity ? Does the effectiveness of suction as a method for delaying transition depend on where it is applied, or on its intensity ? Finally, if the boundary layer would be kept laminar with the least possible suction, then should one allow for a limited growth of the secondary disturbance, or should one increase suction to fully stabilize the secondary disturbance ? The focus of this paper is to answer these questions as well as to shed some light on the mechanism by which the suction control the production of the vortical structure of the secondary instability.

## 2. ANALYSIS

### 2.1. The Mean Flow

We consider a 2D boundary-layer flow of an incompressible fluid with inviscid flow field given by $U=U(x)$ and distributed suction given by $v=v_w(x)$ at the wall, where $x$ is the streamwise direction and $y$ is the normal direction. The flow is governed by the nonsimilar boundary-layer equation

$$f_{\eta\eta\eta}+ff_{\eta\eta}+\hat{\beta}(1-f_{\eta}^{2})-\Gamma f_{\eta\eta} = 2\xi(f_{\xi}f_{\xi\eta}-f_{\xi}f_{\eta\eta}) \tag{1}$$

with boundary conditions

$$f_{\eta}(\xi,0)=0, \quad f(\xi,0)+2\xi f_{\xi}(\xi,0)=0, \quad f_{\eta}(\xi,\eta\to\infty)=1 \tag{2}$$

given in the Gortler variables

$$d\xi=U_e dx, \quad d\eta=(U_e/\sqrt{2}\xi)dy \tag{3}$$

Then the velocity components $u$ and $v$ in terms of the new variables are

$$u=U_e f_{\eta} \tag{4}$$

$$v=v_w-(U_e/\sqrt{2}\xi)\left[f+2\xi f_{\xi}+\eta(\hat{\beta}-1)f_{\eta}\right] \tag{5}$$

where the suction and pressure gradient functions $\Gamma$ and $\hat{\beta}$ respectively are defined as

$$\Gamma(\xi)=(\sqrt{2}\xi/U_e)v_w(\xi) \tag{6}$$

$$\hat{\beta}(\xi)=(2\xi/U_e^2)(dU_e/dx) \tag{7}$$

Note that negative $\Gamma$ indicates suction, while negative $\hat{\beta}$ indicates unfavorable pressure gradient. If both the suction and pressure gradient functions are constant (equal to $\Gamma_0$ and $\beta_0$ respectively), then $f(\xi,\eta)$ is a function of $\eta$ only and we have a similar boundary-layer profile governed by

$$f_{\eta\eta\eta}+ff_{\eta\eta}+\beta_0(1-f_\eta^2)-\Gamma_0 f_{\eta\eta}=0 \tag{8}$$

$$f(0)=f_\eta(0)=0, \quad f_\eta\to 1 \ as\ \eta\to\infty \tag{9}$$

where the condition $\Gamma_0$=*constant* demands that $v_w$ be proportional to $U_e/\sqrt{2\xi}$. On a flat plate, $v_w$ is proportional to $1/\sqrt{x}$ .

## 2.2. The Primary Instability

We consider the primary instability of the calculated mean flow with respect to 2D quasi-parallel spatially growing TS waves. Dimensionless quantities are introduced to the governing incompressible Navier-Stokes equations by using the reference velocity $U_e$ and the reference length $L=(\nu_e x/U_e)^{1/2}$ so that Reynolds number is given by $R=(U_e x/\nu_e)^{1/2}$ where $x$ measures the distance from the leading edge, and $\nu$ is the fluid kinematic viscosity. The primary TS wave is assumed to take the traveling form

$$q(x,y,t)=A\,[q_1(y)\exp(i\int\alpha_r dx-i\omega t)+cc.]+O(A^2) \tag{10}$$

where

$$A\equiv A(x)=A_0\exp(-\int\alpha_i\,dx), \tag{11}$$

and $q_1$ stands for the velocities $u_1$ and $v_1$, and the pressure $p_1$ of the primary wave, and cc denotes complex conjugate. The spatial stability analysis is chosen for being more appropriate for this study. Hence, the wavenumber is complex and given by $\alpha=\alpha_r+i\,\alpha_i$ and the disturbance frequency $\omega$ is real. The linearized incompressible Navier-Stokes equations reduce to a fourth-order system of ordinary differential equations with homogeneous boundary conditions

in $u_1$ and $v_1$. These equations may be combined to yield the well known Orr-Sommerfeld equation. The eigensolutions of the primary wave are normalized such that the amplitude $A$ measures directly the maximum root mean square value of the disturbance velocity in the flow direction. For the purpose of comparison we follow Herbert [20] and let

$$\max_{0\le y\le\infty} 2[u_1(y)]^2 = 1 \tag{12}$$

The linear stability theory of the primary wave provides $\alpha$ for a given $\omega$ and $R$. Then the integration of the growth rate $-\alpha_i$ gives the amplification factor $\ln(A/A_0)$, where $A_0$ is an arbitrary initial amplitude at the onset of the primary instability.

### 2.3. The Secondary Instability

We consider a basic state $\hat{q}(x,y,t)$ which consists of a 2D quasi-parallel boundary layer with pressure gradient and suction modulated by a periodic component of the linear primary instability problem,

$$\hat{q}(x,y,t) = q_0(x,y)+A\ q_1(x,y,t) \tag{13}$$

To study the linear 3D instability of the basic state $\hat{q}(x,y,t)$, we superpose a small unsteady disturbance on each flow quantity of the basic state, that is

$$q(x,y,z,t) = \hat{q}(x,y,t) + B\ q_2(x,y,z,t) \tag{14}$$

where $q_2$ is a secondary disturbance eigenfunction that stands for velocities $u_2$, $v_2$, $w_2$, and pressure $p_2$, they are normalized such that the amplitude $B$ measures the maximum root mean square value of $u_2$. The amplitude $B$ is assumed small compared to the primary amplitude $A$, such that the primary instability will influence the secondary instability but not vice versa.

Herbert [22] has pointed out that the 3D secondary instability occurs at small amplitudes of the primary wave where the nonlinear distortion is weak. This instability is of vortical nature and originates from a strong mechanism of combined tilting and stretching of the vortices [5], leading to large growth rates when compared with those for the primary wave. In

view of that, we neglect in this analysis the nonlinear distortion of the eigensolutions $q_1$ at finite amplitude of the primary wave. Also, the growth of the primary TS wave which occurs on viscous scales can be considered weak, and the variation of the primary amplitude $A$ can be assumed locally constant.

Equation (14) is substituted into the dimensionless Navier-Stokes equations. The basic state is subtracted, and the resulting equations are linearized with respect to the secondary amplitude $B$. We end up with four coupled partial differential equations for the secondary 3D instability. The coefficients of these equations are function of the basic state, they are independent of the coordinate $z$, and periodic in $x$ and $t$. Hence, the $z$-variation can be separated, and Floquet theory of differential equations with periodic coefficients can be applied to give a solution in the form

$$q_2(x,y,z,t) = e^{\gamma x+\sigma t} e^{i\beta z}\ \hat{\phi}(x,y,t) \tag{15}$$

where $\beta$ is a real spanwise wavenumber of the secondary disturbance. $\gamma=\gamma_r+i\gamma_i$ and $\sigma=\sigma_r+i\sigma_i$ are two complex characteristic exponents, and $\hat{\phi}(x,y,t)$ is a periodic function of $(x-\omega t/\alpha)$, the same as the period of the basic state. We express $\hat{\phi}$ in terms of Fourier series to obtain the following expression for $q_2$

$$q_2(x,y,z,t) = e^{\gamma x+\sigma t} e^{i\beta z} \sum_{n=-\infty}^{\infty} \phi_n(y)\ e^{in\alpha(x-\omega t/\alpha)} \tag{16}$$

Equation (16) represent the general Floquet form for the eigenmodes of a periodic basic state, where both the fundamental and subharmonic modes are special cases. Only two of the four real exponents $\gamma_r$,$\gamma_i$, $\sigma_r$, and $\sigma_i$, are determined as a solution of the eigenvalue problem, others must be given. For the purpose of our study of the spatial instability of subharmonic modes, we let $\gamma_r$ represent the growth rate of the secondary instability, $\sigma_r$=0 (no temporal growth), $\sigma_i$=$-\omega/2$ for pure subharmonic mode, and let $\gamma_i$ represent the shift in the streamwise wavenumber of the secondary disturbance with respect to the primary one. $\gamma_i$=0 means that the secondary disturbance is perfectly synchronized with the basic state.

We use the lowest truncation of the Fourier series for the subharmonic mode ($n \leq 1$) in Eq (16), to derive four coupled ordinary differential equations for $u_2$, $v_2$, $w_2$, and $p_2$. These equations when supplemented with homogeneous boundary conditions, they constitute an eigenvalue problem

$$\gamma = \Gamma(\alpha, \beta, R; A) \tag{17}$$

for a given boundary-layer velocity profile with pressure gradient and suction. The eigenvalue problem (17) of the secondary instability provides $\gamma$ for a given $\beta$ and $R$. Then the integration of the growth rate $\gamma_r$ gives the amplification factor $\ln (B/B_0)$, where $B_0$ is an arbitrary initial amplitude at the onset of the secondary instability.

## 3. NUMERICAL TREATMENT

Similar boundary layer profiles were calculated using Eqs (8)-(9). These equations were numerically integrated by using a shooting technique with fourth-order Runge-Kutta and Adams-Moulton integrator. In cases of continuous suction, where $v_w$ = constant, similar solutions do not exist, and Eqs (1)-(2) were numerically integrated by using a step by step procedure in the streamwise direction. A three-point implicit finite difference technique was used to reduce them to a set of simultaneous tridiagonal equations. These equations were linearized and then solved using the algorithm of Thomas. The method of solution closely parallel that of Price and Harris [24].

The primary instability which modulate the 2D boundary layer is governed by a fourth-order system of equations. While the eigenvalue problem (17) describing the secondary disturbance, is governed by a sixth-order system of equations. Both can be written as complex system of linear first-order ordinary differential equations in the form

*Primary*

$$DZ_{1n} - \sum_{m=1}^{4} a_{nm} Z_{1m} = 0, \quad n=1,2..4 \tag{18}$$

$$Z_{11} = Z_{13} = 0 \qquad at \quad y=0 \tag{19}$$

$$Z_{11}, Z_{13} \to 0 \qquad as \quad y \to \infty \tag{20}$$

where $Z_{1n}$ are defined by

$$Z_{11} = u_1, \quad Z_{12} = Du_1, \quad Z_{13} = v_1, \quad Z_{14} = p_1$$

*Secondary*

$$DZ_{2n} - \sum_{m=1}^{6} b_{nm} Z_{2m} = A \sum_{m=1}^{6} c_{nm} \bar{Z}_{2m}, \quad n=1,2..6 \tag{21}$$

$$Z_{21} = Z_{23} = Z_{25} = 0 \qquad at \quad y=0 \tag{22}$$

$$Z_{21}, Z_{23}, Z_{25} \to 0 \qquad as \quad y \to \infty \tag{23}$$

where $Z_{2n}$ are defined by

$$Z_{21} = u_2, \quad Z_{22} = Du_2, \quad Z_{23} = v_2,$$

$$Z_{24} = p_2, \quad Z_{25} = w_2, \quad Z_{26} = Dw_2$$

and the overbar denotes a complex conjugate. The $a_{nm}$ are the elements of 4x4 variable coefficient matrix of the primary eigenvalue problem, while $b_{nm}$ and $c_{nm}$ are the elements of 6x6 variable coefficient matrices of the secondary eigenvalue problem. These elements are given in the Appendix. Note that in case of no modulation of the mean flow by a primary wave (*i.e.* $A=0$), then the system of equations (21)-(23) will govern the stability of a primary subharmonic 3D wave.

Both the primary and secondary system of equations are numerically integrated as initial value problem using a freestream solution as initial condition. For the secondary eigenvalue problem, we assume that the amplitude of the primary vanishes far in the freestream at $y \geq y_e$ (e denotes the edge of the boundary layer). Then the system (21) will have constant coefficients and can be solved analytically producing three linearly independent exponentially decaying solutions to conform with the boundary condition (23). With the freestream solution as initial condition, Eqs (21) are integrated from $y=y_e$ to $y=0$ at the wall, using a variable step-

size algorithm [25], based on the Runge-Kutta-Fehlburg fifth-order formulas. The solution is orthonormalized at a preselected set of points using a modified Gram-Schmidt procedure. A Newton-Raphson technique is used to iterate on the eigenvalue to satisfy the last wall boundary condition within a specified accuracy of $O(10^{-5})$.

## 4. RESULTS AND DISCUSSION

For the Blasius and Falkner-Skan profiles, our results were checked with that of Bertolotti [26], and found to be in full agreement.

All results reported here are for the nondimensional frequency $F=10^6\omega/R=60$, that remains fixed as a wave with fixed physical frequency travels downstream. For Blasius flow, a primary TS wave with this frequency grows between $R_I\approx554$ and $R_{II}\approx1052$ (first and second neutral stability points), reaching a maximum amplification factor of $A/A_0\approx42$. Also in this region, primary 3D subharmonic waves are subject to amplification for a broad band of spanwise wavenumbers, but the time and length scales of these instabilities are too small to compare with experimentally observed transition. A strong growth of secondary 3D subharmonics can be due to parametric excitation by the finite amplitude primary TS wave [20].

### 4.1. Flat Plate Boundary Layer Controlled by Suction

At $R=1050$ ( almost at $R_{II}$ for Blasius flow), Fig (1) shows the growth rates of the secondary 3D subharmonic disturbances as function of the spanwise wavenumber parameter $b$ and for various amplitudes $A$ of the primary wave. The parameter $b$ defined as $b=10^3\beta/R$ represents a fixed physical spanwise wavenumber for a wave traveling downstream. Figure (1) compares the results of a flat plate boundary layer with suction ($\Gamma_0=-.1$) and with no suction. At fixed $\Gamma_0$, the figure indicates a stabilizing effect on the secondary instability as the primary amplitude $A$ decreases. When the amplitude is very small, considerable growth rates exist in a small band of spanwise wavenumbers. The maximum growth occurs for a wave with slightly lower spanwise wavenumber as the amplitude $A$ decreases. This shift to lower spanwise

wavenumber is more noticeable with the increase of suction parameter. As Reynolds number increases, the growth rates of the secondary disturbances increase at fixed $F$ and $A$.

The application of active control by suction in LFC systems restrains both the mean-flow profile and the primary wave. We find that the prime influence of suction on the secondary instability is due to the appreciable decay of the amplitude of the primary wave. This conclusion is explained next with the use of Fig. (2). In Blasius flow, a primary wave with initial amplitude $A_0$ =0.00025 at $R_I$ grows such that at $R$ =1050 downstream its amplitude reaches a value of 0.01. Figure (2), curve a, shows a wide band of 3D subharmonics amplifying at that location with the most unstable at $b = 0.17$. The influence of a modified mean flow can be demonstrated by applying suction at $R$ = 1050 with fixed $A$=0.01. This decreases the growth rate of the subharmonic and slightly limit the band of amplified spanwise wavenumbers (curves b and c), while the most unstable wavenumber is not affected by suction. When suction is applied ( $\Gamma_0 = -0.05$) starting upstream at $R_I$, the mean flow is modified and the growth of the primary wave is slowed down, such that at $R$ = 1050 downstream the amplitude of the primary wave reaches a value of 0.0015. Calculations, curve d, indicate a strong stabilizing effect on the secondary instability with the most unstable 3D subharmonic occurring at a lower spanwise wavenumber.

Previous results may be viewed as local, they only reflect the stability characteristics of the secondary subharmonic disturbance at a fixed Reynolds number. To model the experiment and evaluate the overall effect of suction on the onset, growth rate, and amplification factor of the secondary 3D subharmonic, we should combine the effect of increasing the amplitude $A$ of the primary TS wave as well as increasing $R$ as the disturbance moves downstream. In Fig (3), we do that and show the variation with $R$ of the growth rates of the secondary subharmonic wave. In these calculations, the initial amplitude of the primary wave is assumed $A_0$=.001, and the spanwise wavenumber $b$=.15 which is an average value of the most unstable wavenumbers for the parameters under investigation. The growth rates of the corresponding primary waves are also included in the figure for comparison.

The micro-events which lead to the secondary 3D instability go as follows. Initially, the primary instability sets in at $R_I$ on the primary neutral curve, and $-\alpha_i$ starts to grow. At a certain value of the primary amplitude, a secondary 3D mode is induced and sets in at $R_I$ on a secondary neutral curve. $\gamma_r$ starts to grow strongly due to the increase in both $A$ and $R$. Ultimately, $-\alpha_i$ begins to decay, and the primary amplitude reaches a maximum when $-\alpha_i=0$. Shortly downstream, $\gamma_r$ reaches a maximum and then starts to decay with the secondary amplitude reaching its maximum when $\gamma_r=0$. The overall effect of small suction rates is to delay the onset of the secondary instability (occurs later downstream), and to decrease significantly its growth rate. Calculated amplification factors for the secondary disturbance (not shown) indicate 71 % reduction due to the increase of $\Gamma_0$ from 0 to -.05. Increasing $\Gamma_0$ to -.1 dampened completely the subharmonic secondary disturbance in spite of considerable growth shown by the primary wave. We know from the experiment [9] that the secondary instability depends on the primary wave amplitude as well as on the wave fetch. In a fixed disturbance environment, small suction rates may not affect the initial amplitude of the primary wave but certainly will influence its growth. Our calculations in Fig (3) indicate a delay in the onset of the secondary instability due to suction. This delay is accompanied by a slight decrease in the primary threshold amplitude (equal to .0029 at $\Gamma_0=0$ and .0024 at $\Gamma_0=-.05$). However, at $\Gamma_0=-.1$, the primary amplitude reaches a maximum of only .0014 which is apparently below the value needed to induce a secondary subharmonic instability. Notice that the initial amplitude of the primary wave is fixed in all cases and equal to .001.

Figure (4), a case of suction rate $\Gamma_0=-.05$, shows a primary instability that sets in at $R=650$. The onset of the subharmonic instability occurs at $R=850$ when $A_0=.001$, at $R=775$ when $A_0=.002$, and at $R=635$ when $A_0=.0066$ (which is well before the onset of the primary wave), reaching maximum amplification factors of 8, 15, and 30 respectively. Note that when the initial amplitude $A_0$ is large enough, the induced instability can be so strong and secondary instability occurs directly by-passing the usual growth of the primary wave. In a situation like this, transition prediction schemes based on linear primary theory fail completely.

In boundary-layer flows, the onset of the secondary 3D instability is known to be an important feature of the early stages leading to transition. For LFC purposes, one might try to completely avoid or delay this instability by using suction. Then, one faces questions like where to apply suction, and whether it should start before or after the onset of the secondary instability, and what is the optimum suction needed to keep the flow laminar. To answer these questions, calculations were made to compare the stability characteristics of different cases of Blasius flow with continuously applied suction starting at five different locations. These results are reported in Fig (5) which shows the variation with $R$ of the growth rates of both the primary and secondary disturbances at fixed initial amplitude of the primary wave ($A_0$=0.001). Calculations show that in order to control the secondary 3D instability, suction should be applied further upstream near $R_I$ of the primary wave and not to apply it near the onset of the secondary instability. While investigating the effect of suction on primary TS waves, Reed and Nayfeh [27] and Saric and Reed [28] reached similar conclusions that suction should be concentrated not in the region of maximum growth but near its first neutral stability.

Figure (6) shows the variation with suction parameter $\Gamma_0$ of the maximum growth rates with respect to $R$ of both the primary wave and secondary subharmonic disturbance for $A_0$=.001 and $b$=.15. Point P indicates a suction level that completely stabilizes the primary wave, while point S indicates a suction level that allows for a limited primary growth but completely stabilizes the secondary disturbance ( point S is extrapolated due to doubtful Floquet theory results when the secondary growth rates are small). An optimum suction requirements for an LFC system may be located somewhere upstream of point S allowing for a considerable growth of the most unstable primary wave, as well as a limited growth of the secondary disturbance as long as the primary amplitude is small and the induced secondary disturbance is not strong enough for nonlinear self- and cross-interaction with the primary wave. As $A_0$ increases, point S is expected to move towards point P and cross it over for high enough primary initial amplitudes. In such situation, suction level required to fully stabilize the primary wave may not control the amplification of the secondary disturbance, and very high suction levels are needed

to control the flow.

### 4.2. Falkner-Skan Flow Controlled by Suction

The need to control the secondary instability in a boundary layer with pressure gradient is more realistic such as the case of flow on airfoils. Herbert and Bertolotti [29] studied the secondary instability of Falkner-Skan flows and found that favorable pressure gradient limits the band of unstable spanwise wavenumbers, while small adverse pressure gradient is strongly destabilizing. This means that larger suction rates are needed to control the boundary layer in these cases. For a boundary layer with pressure gradient and suction, the variation of the growth rates of the secondary 3D subharmonic with the spanwise wavenumber parameter $b$ exhibits the same features given before in Fig(1).

Figure (7) gives an overall view of the effect of both pressure gradient and suction parameters on the secondary 3D subharmonic at fixed $A_0$ using the maximum amplification factor as a basis for comparison. As adverse pressure gradient increases, the secondary subharmonic disturbance becomes more unstable. With the suction parameter increasing, the curves converge rapidly to lower amplification factors indicating that the secondary instability is more sensitive to suction as adverse pressure gradient increases. Figure (7) shows also the increase in the maximum amplification factors for different values of $A_0$ at $\beta_0$=0. The sensitivity of the secondary instability to suction appears to be higher with the increase in adverse pressure gradient than the increase in $A_0$.

### 4.3. Mean Profile, Mode Shape, and Vortical Structure

Modifications to the Blasius profile due to suction and adverse pressure gradient are shown in Fig (8). Suction leads to a fuller mean $U$-velocity profile and decrease in the magnitude of the $V$-velocity. While adverse pressure gradient makes the $U$-velocity profile more inflectional. At fixed amplitude of the primary wave, these modifications have moderate effect on the secondary instability, see Fig (2) for the case of suction, and Ref. 27 for the case of

pressure gradient.

Figure (9) gives a comparison of the mode shapes of the $u$-, $v$-, and $w$-velocity components of the secondary disturbance at different suction and pressure gradient parameters. The $v$-component is small and is slightly affected by suction or pressure gradient. The corresponding mode shapes of the $u$- and $v$-velocity components of the primary wave are shown in Fig (10) for comparison. Suction tends to move the critical layer closer to the wall with the maximum of the primary wave velocity components and the maximum of the secondary disturbance velocity components following it. The location of the critical layer on the $\eta$-axis is marked in both figures. By increasing suction, the thickness of the boundary layer decreases, and the disturbance is confined to a region closer to the wall where dissipative action is strong, thereby increasing the stability of the flow. As adverse pressure gradient increases, the opposite occurs and a change over from viscous to inflectional instability takes place [29].

A more detailed description of the physics of the process of suction control can be obtained from contour plots of the vorticity components. Figures (11)-(14) give contours of vorticity components in a wave-fixed coordinate system for different cases of suction and pressure gradients at $R$=1050. In each figure, frames (a)-(d) show the effect of the mean-flow modification on the vorticity contours ($A$=0.04 and $B$=1 are fixed), while frame (e) shows the total effect of the suction on the vorticity contours due to modifications in the mean flow and the reduction in the primary amplitude ($A$=0.006 and $B$=0.005). These values of $A$ and $B$ are calculated at $R$=1050 assuming $A_0$=0.001 at the onset of the primary wave, and $B_0$=1x10$^{-6}$ at the onset of the secondary subharmonic. Comparison of frames (a) and (d) in each figure shows that suction with $\Gamma_0$=−.2 applied to an inflectional profile with $\beta_0$=.19 qualitatively produces the same vorticity contour plots as for a blasius profile.

An array of streamwise-periodic concentrations of vorticity is established by the primary viscous instability. The strength of the vorticity intensifies with the increase of the amplitude of the primary wave. Figure (11) shows plots of the initial 2D vorticity contours of the basic

flow ( only spanwise component exist). which peaks near the wall, and extends to the critical layer. The location of the critical layer is defined by tick marks on the $\eta$-axis.

With the onset of the secondary instability, 3D vortical structure is induced by the deformation of the initial 2D vorticity. Figure (12) shows plots of the spanwise vorticity $\zeta_z$-contours in the $x-y$ plane at $z=0$ for different cases of suction and pressure gradient. The figure that is plotted over four primary wavelengths ($\lambda_x=2\pi/\alpha$), indicates that regions of concentrated spanwise vorticity are convected downstream, pulled towards the wall as suction increases, and lifted away from the wall as adverse pressure gradient increases. In both situations, the concentrated vorticity follows the critical layer as the suction and/or pressure gradient changes.

The spanwise-velocity variations produce streamwise vorticity $\zeta_x$ that is contoured in Fig (13). The figure is plotted in the $z-y$ plane at $x=0$ over two spanwise wavelengths of the secondary disturbance ($\lambda_z=2\pi/\beta$). It shows an array of counter-rotating vortices extending away from the wall as adverse pressure gradient increases, and pulled towards the wall as suction increases.

Following the onset of the secondary instability, spanwise and streamwise vortices experience a process of stretching and tilting as they move downstream. Together, they form a large scale 3D structure ( $\Lambda$-shaped) which was observed experimentally and numerically. For different suction and pressure gradient parameters, Fig (14) shows the deformation in the total vorticity ($\sqrt{\zeta_x^2+\zeta_z^2}$) in an $x-z$ plane almost at the $\eta$-location of the critical layer.

## 5. CONCLUDING REMARKS

Calculations show that the secondary 3D subharmonic instability is very sensitive to and can be controlled by suction. Meaning, the onset of the instability is delayed, the growth rates and amplification factors are reduced, the unstable band of spanwise wavelengths is limited, and the vortical structure is closer to the wall. As adverse pressure gradient increases, the sensitivity to suction increases. For higher initial amplitude of the primary wave, suction is less effective in controlling the secondary 3D subharmonic instability.

Calculations show that elimination of the primary wave by suction at an arbitrary stage of its growth might not delay or eliminate the secondary instability specially if it has already taken place. The suction need be applied near $R_I$ of the primary wave to gain more control on the secondary growth. An optimum suction amount may be lower or higher than the suction needed to fully eliminate the primary wave. This is very much dependent on the initial amplitude of the primary wave.

Application of suction influences both the mean profile and the primary wave. The effect of a modified mean profile on the secondary 3D instability is moderate, while the main effect is due to enhancing the growth of the primary wave. By applying suction and including both effects, calculations indicate that the most unstable secondary subharmonic disturbance occurs at lower spanwise wavenumber. Then, at certain downstream location, an observed flow structure of the H-type might be altered to C-type with larger spanwise wavelength or might completely disappear as suction increases.

Evaluation of the effect of suction on the subharmonic secondary instability is a step towards the goal of optimizing an LFC system. The idea of monotoring the 3D $\Lambda$-shaped structure as its spanwise wavelength changes with suction may be used for that purpose.

## ACKNOWLEDGEMENT

This work was supported by NASA Langley Research Center, under contract NAS1-18599.

## APPENDIX : Nonzero Elements of the Coefficient Matrices $a_{nm}$, $b_{nm}$, and $c_{nm}$ of Eqs (18) and (21) :

$$a_{12} = 1, \quad a_{21} = iR(\alpha U - \omega) + \alpha^2, \quad a_{23} = R\ DU\ , \quad a_{24} = i\alpha R\ ,$$

$$a_{31} = -i\alpha\ , \quad a_{42} = -i\alpha/R\ , \quad a_{43} = -i(\alpha U - \omega) - \alpha^2/R$$

$$b_{12} = 1\ , \quad b_{21} = 1\ , \quad b_{23} = RDU\ , \quad b_{26} = (\gamma + \frac{1}{2} i\alpha_r)R\ ,$$

$$b_{31} = -b_{26}/R \ , \quad b_{34} = -\beta \ , \quad b_{45} = 1$$

$$b_{54} = (\gamma + \frac{1}{2} i \alpha_r) U - \frac{1}{2} i \omega) R - (\gamma + \frac{1}{2} i \alpha_r)^2 + \beta^2$$

$$b_{56} = -R \ \beta \ , \quad b_{62} = b_{31}/R \ , \quad b_{63} = -b_{54}/R \ , \quad b_{65} = -\beta/R \ ,$$

$$c_{21} = (\gamma + \frac{1}{2} i \alpha_r) R u_1 \ , \quad c_{22} = R v_1 \ , \quad c_{23} = R \ D u_1 \ , c_{54} = (\gamma - \frac{1}{2} i \alpha_r) R u_1 \ ,$$

$$c_{55} = R \ v_1 \ , \quad c_{61} = (\gamma - \frac{3}{2} i \alpha_r) v_1 \ , \quad c_{63} = -c_{54}/R - D v_1 \ , \quad c_{64} = \beta v_1$$

## REFERENCES

1. W. D. Harvey and J. D. Pride, The NASA Langley Laminar Flow Control Experiment. AIAA Paper 82-0567 (1982).

2. J. N. Hefner and D. M. Bushnell, Application of Stability Theory to Laminar Flow Control. AIAA Paper 79-1493(1979).

3. W. S. Saric, Laminar Flow Control with Suction: Theory and Experiment. AGARD Report No. 723 (1985).

4. I. Tani, Three-Dimensional Aspects of Boundary-Layer Transition. In Proceedings of Indian Academy of Science 4, 219 (1981).

5. S. A. Orszag and A. T. Patera, Secondary Instability of Wall-bounded Shear Flows. J. Fluid Mech. 128, 347 (1983).

6. Th. Herbert, Secondary Instability of Plane Channel Flow to Subharmonic Three-Dimensional Disturbances. Phys. Fluid 26, 871 (1983).

7. P. S. Klebanoff, K. D. Tidstrom, and L. M. Sargent, The Three Dimensional Nature of Boundary Layer Instability. J. Fluid Mech. 12, 1 (1962).

8. L. S. G. Kovasznay, H. Komoda, and B. R. Vasudeva, Detailed Flow Field in Transition. In Proc. Heat Transfer and Fluid Mech. Institute, Stanford University Press, 1-26 (1962).

9. Yu. S. Kachanov and V. Ya Levchenko, Resonant Interactions of Disturbances in Transition to Turbulence in a Boundary Layer. J. Fluid Mech. 138, 209 (1984).

10. W. S. Saric and A. S. W. Thomas, Experiments on the Subharmonic Route to Transition. In Turbulence and Chaotic Phenomenon in Fluids, ed. T. Tatsumi, North Holland (1984).

11. W. S. Saric, V. V. Koslov, and V. Ya. Levchenko, Forced and Unforced Subharmonic Resonance in Boundary-Layer Transition. AIAA Paper 84-0007 (1984).

12. A. S. W. Thomas, Experiments on Secondary Instabilities in Boundary Layers. In Proc. of 10th US Natl. Congr. Appl. Mech., Austin, Tex, 436-444 (1987).

13. A. Wray and M. Y. Hussaini, Numerical Experiments in Boundary Layer Stability. Proc. Roy. Soc. London A, 392, 373 (1984).

14. T. A. Zang and M. Y. Hussaini, Numerical Experiments on Subcritical transition Mechanisms. AIAA Paper 85-0296 (1983).

15. P. R. Spalart and K. S. Yang, Numerical Study of Ribbon-Induced Transition in Blasius Flow. J. Fluid Mech. 178, 345 (1987).

16. H. F. Fasel, U. Rist, and U. Konzelmann, Numerical Investigation of the Three-Dimensional Development in Boundary Layer Transition. AIAA Paper 87-1203 (1987).

17. T. A. Zang and M. Y. Hussaini, Numerical Experiments on the Stability of Controlled Shear Flows. AIAA Paper 85-1698 (1985).

18. L. Kleiser and E. Laurien, Numerical Investigation of Interactive Transition Control. AIAA Paper 85-0566 (1985).

19. B. Siger, H. L. Reed, and J. H. Ferziger, Effect of Streamwise Vortices on Transition in Plane-Channel Flow. Phys. Fluids A, 1, 1960 (1989).

20. Th. Herbert, Analysis of the Subharmonic Route to Transition in Boundary Layers. AIAA Paper 84-0009 (1984).

21. A. D. D. Craik, Nonlinear Resonant Instability in Boundary Layers. J. Fluid Mech. 50, 393 (1971).

22. Th. Herbert, Secondary Instability of Boundary Layers. Ann. Rev. Fluid Mech. 20, 487 (1988).

23. B. J. Bayly, S. A. Orszag, and Th. Herbert, Instability Mechanisms in Shear-Flow Transition. Ann. Rev. Fluid Mech. 20, 359 (1988).

24. J. M. Price and J. E. Harris, Computer Program for Solving Compressible Nonsimilar Boundary-Layer Equations for Laminar, Transitional, or Turbulent Flows of a Perfect Gas. NASA TM X-2458 (1972).

25. M. R. Scott and H. A. Watts, Computational Solutions of Two-Point Boundary-Value Problems Via Orthonormalization. SIAM J. Num. Analy. 14, 40 (1977).

26. F. P. Bertolotti, Temporal and Spatial Growth of Subharmonic Disturbance in Falkner-Skan Flow. M.S Thesis, VPI&SU, 1985.

27. H. L. Reed and A. H. Nayfeh, Stability of Flow Over Plates with Porous Suction. AIAA Paper 81-1280 (1981).

28. W. S. Saric and H. L. Reed, Effect of Suction and Blowing on Boundary Layer Transition. AIAA Paper 83-0043 (1983).

29. Th. Herbert, and F. P. Bertolotti, Effect of Pressure Gradients on the Growth of Subharmonic Disturbances in Boundary Layers. In Proc. on Low Reynolds Number Airfoil Aerodynamics, Univ. of Notre Dame, ed. T. J. Mueller (1985).

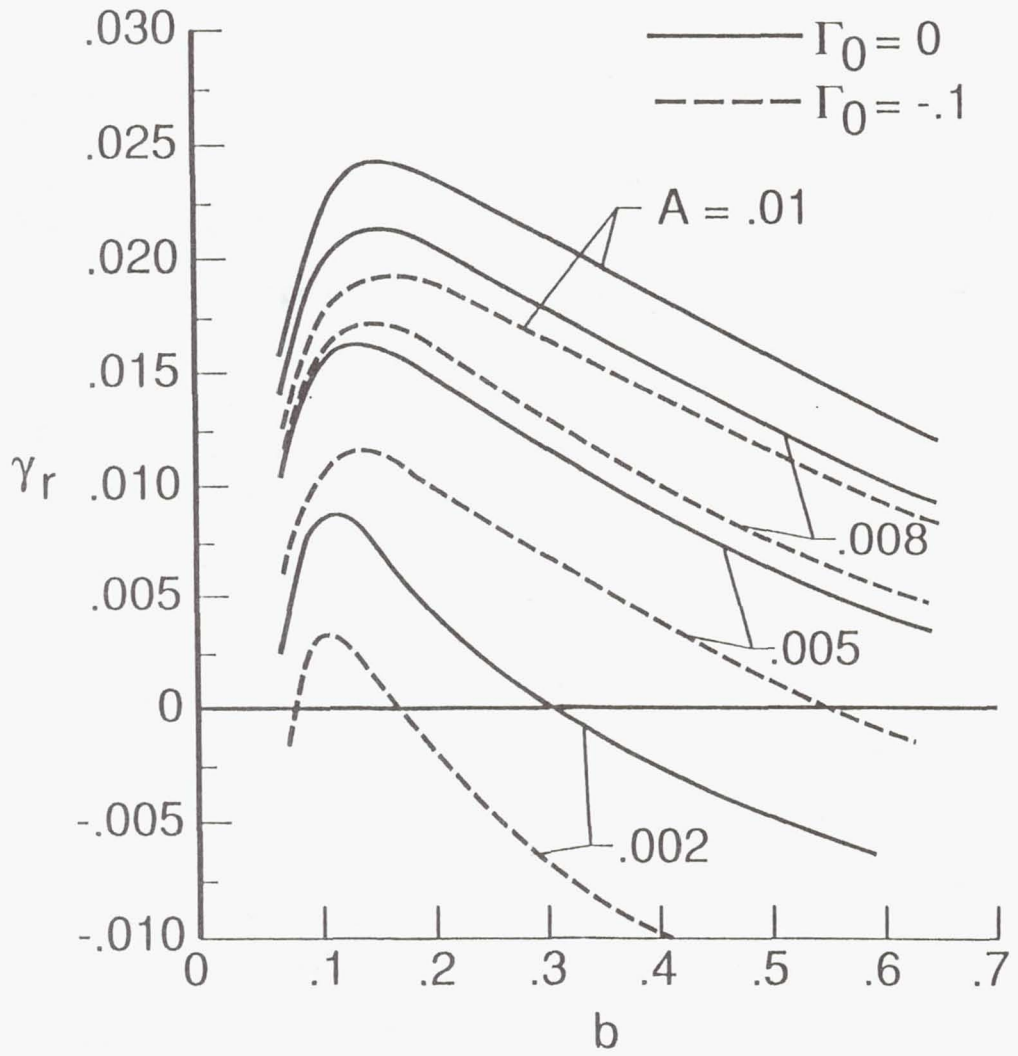


Fig. 1 Effect of the amplitude $A$ of the primary wave on the growth rate of the secondary 3D subharmonic at different suction parameters, $R = 1050$, and $F = 60$.

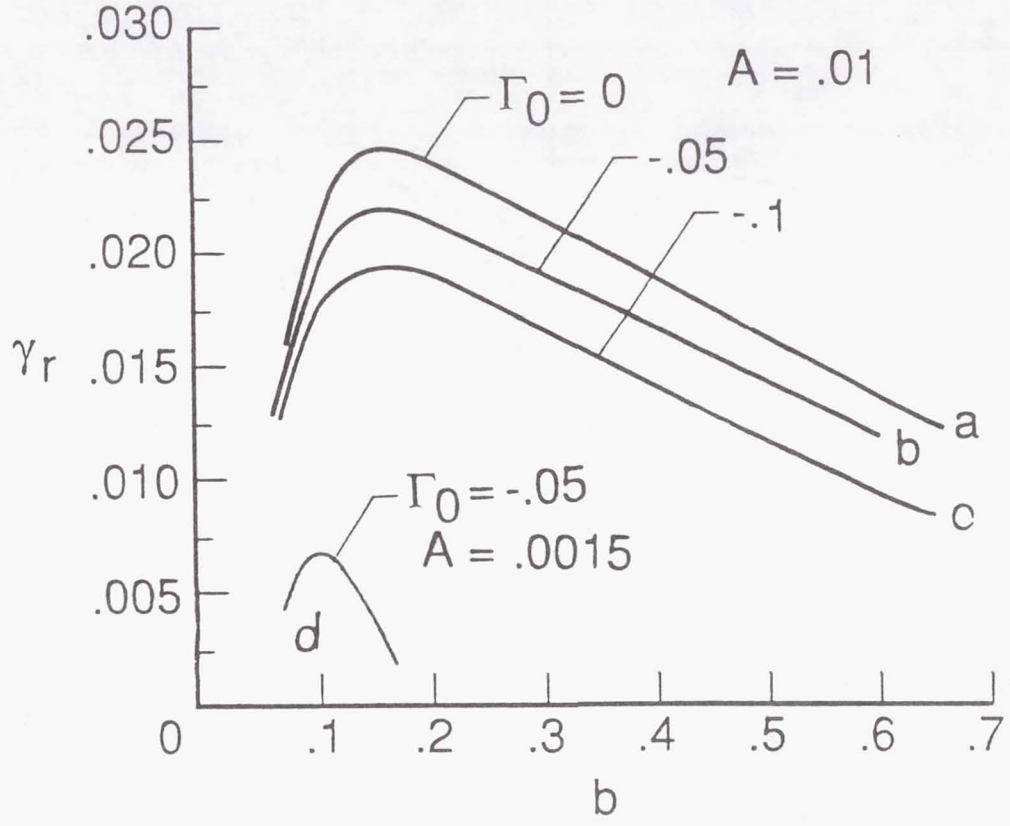


Fig. 2 Effect of mean-flow modifications on the growth rate of the secondary 3D subharmonic at $R = 1050$ ( curves a, b, and c, with fixed $A = 0.01$) and the total effect of suction (on mean flow and primary wave, curve d , with $A = 0.0015$). $A_0 = 0.00025$, and $F = 60$.

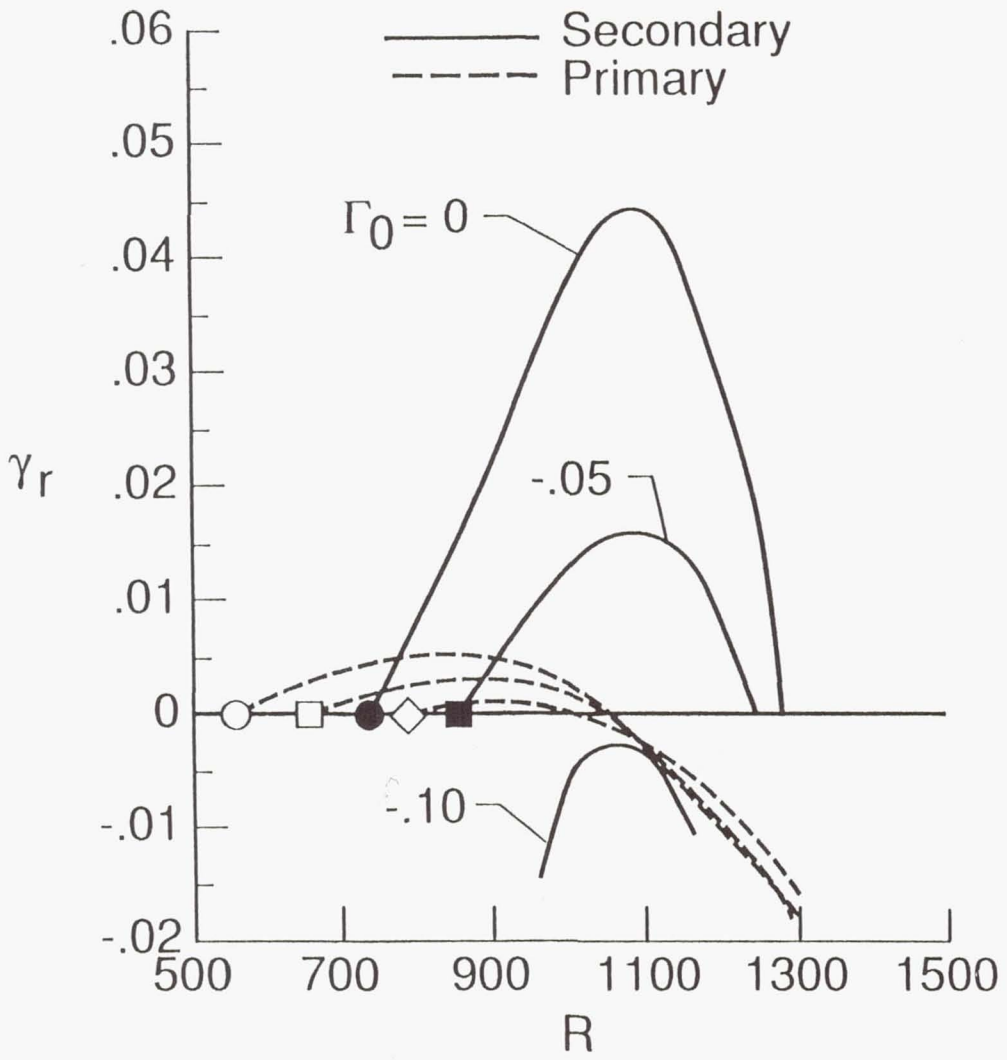


Fig. 3 Effect of suction parameter on the onset and growth rates of the primary wave and secondary 3D subharmonic, $A_0 = .001$, $b = .15$, and $F = 60$.

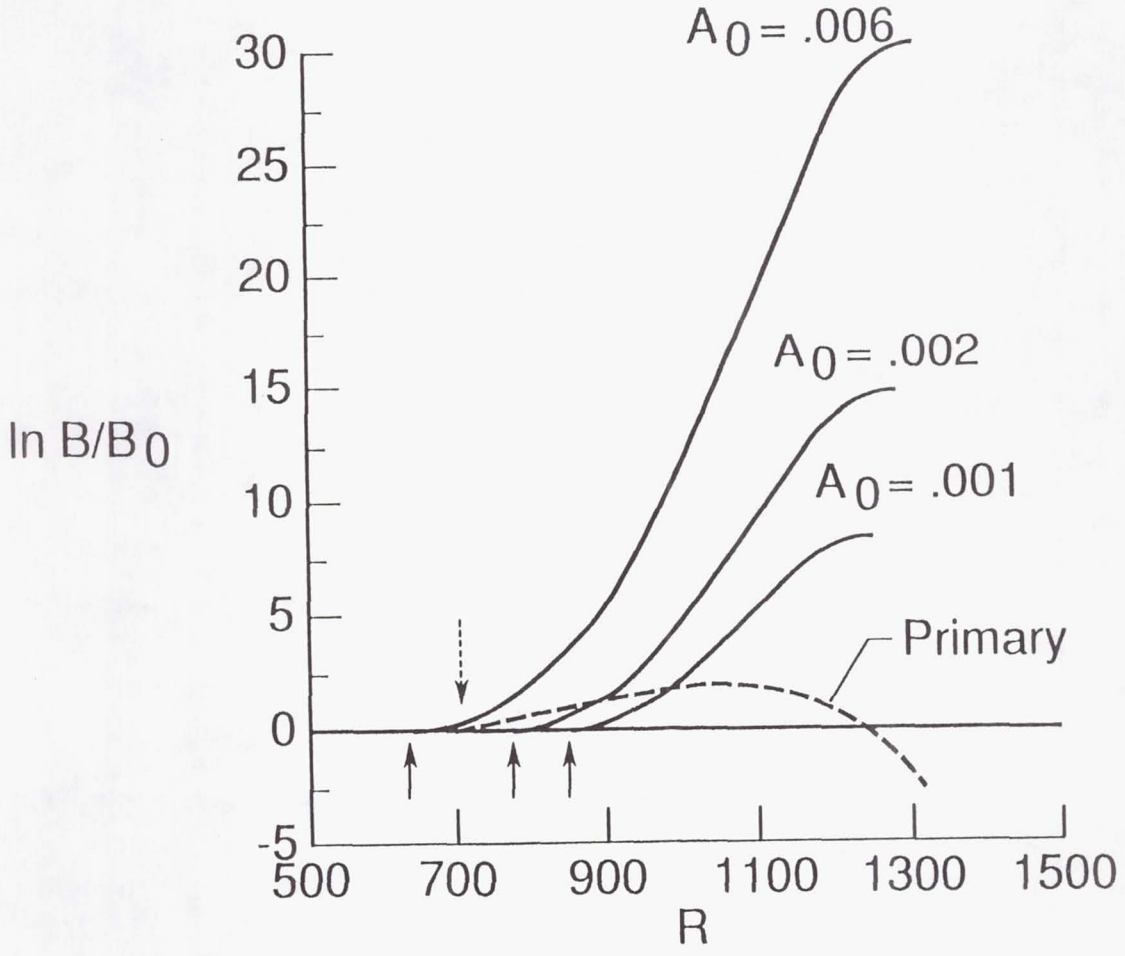


Fig. 4 Effect of the initial amplitude $A_0$ of the primary wave on the onset and amplification factor of the secondary 3D subharmonic, dotted arrow: onset of the primary, solid arrow: onset of the secondary subharmonic, $\Gamma_0 = -.05$, $b = .15$, and $F = 60$.

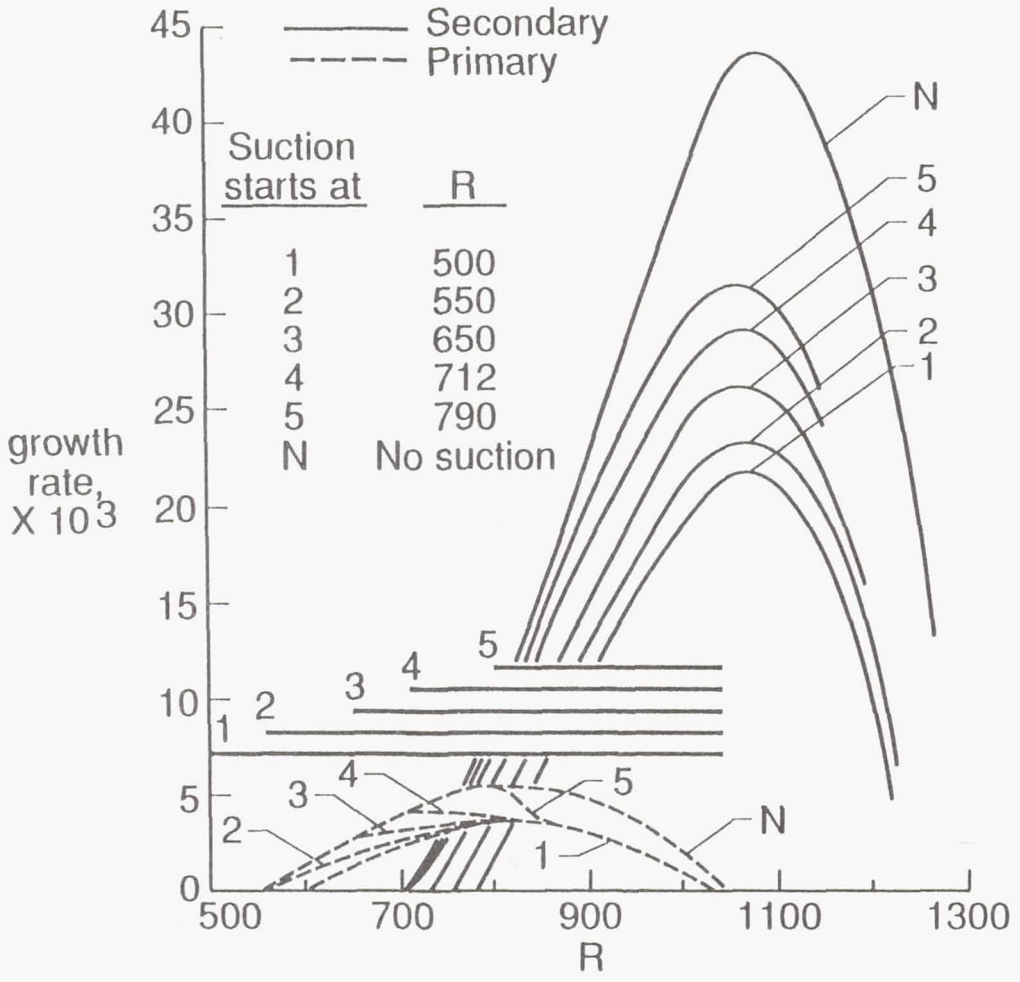


Fig. 5 Continuous suction starting at different locations and its effect on the onset and growth rate of both the primary wave and the secondary 3D subharmonic, $A_0$=.001, $b$=.15, and constant suction level (corresponding to $\Gamma_0 = -.05$ *at* $R = 1000$).

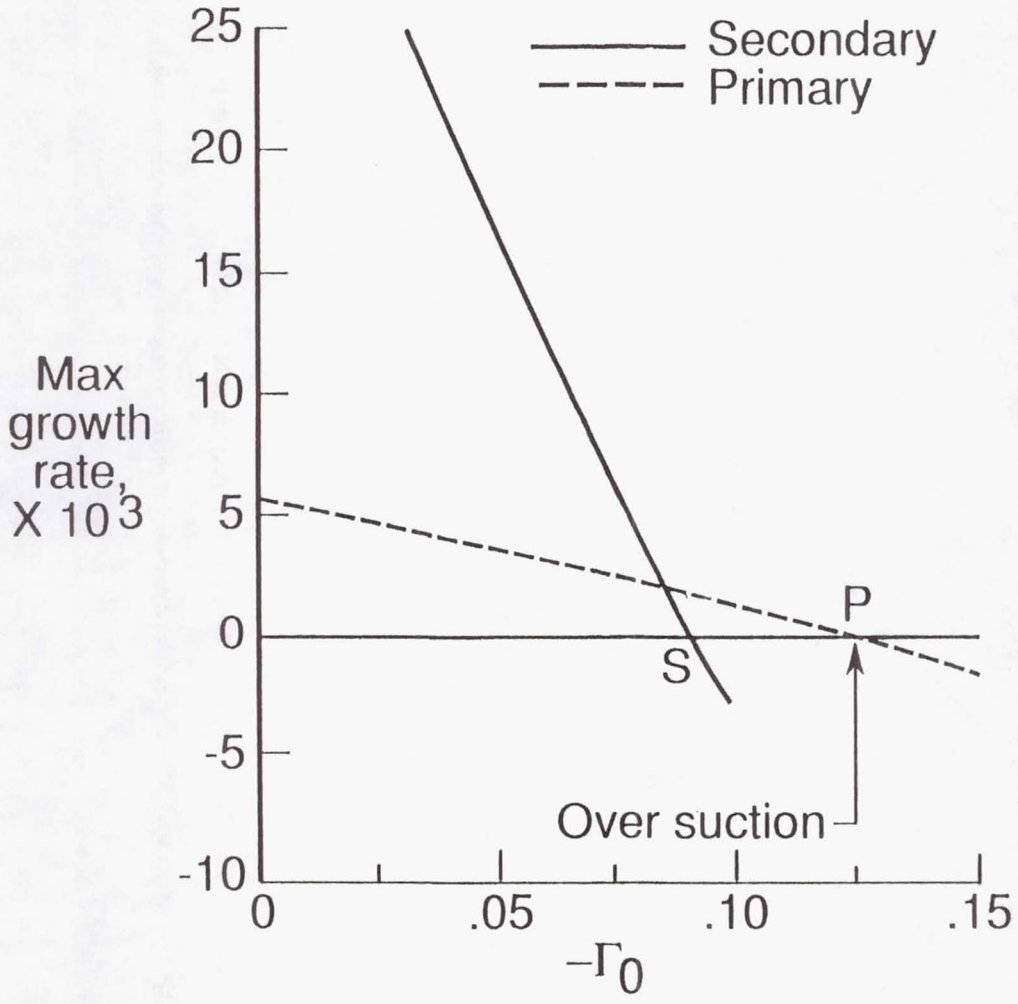


Fig. 6 Variation of maximum growth rate with the suction parameter for both the primary wave and the secondary 3D subharmonic, $A_0$=.001, $b$=.15, and $F$=60.

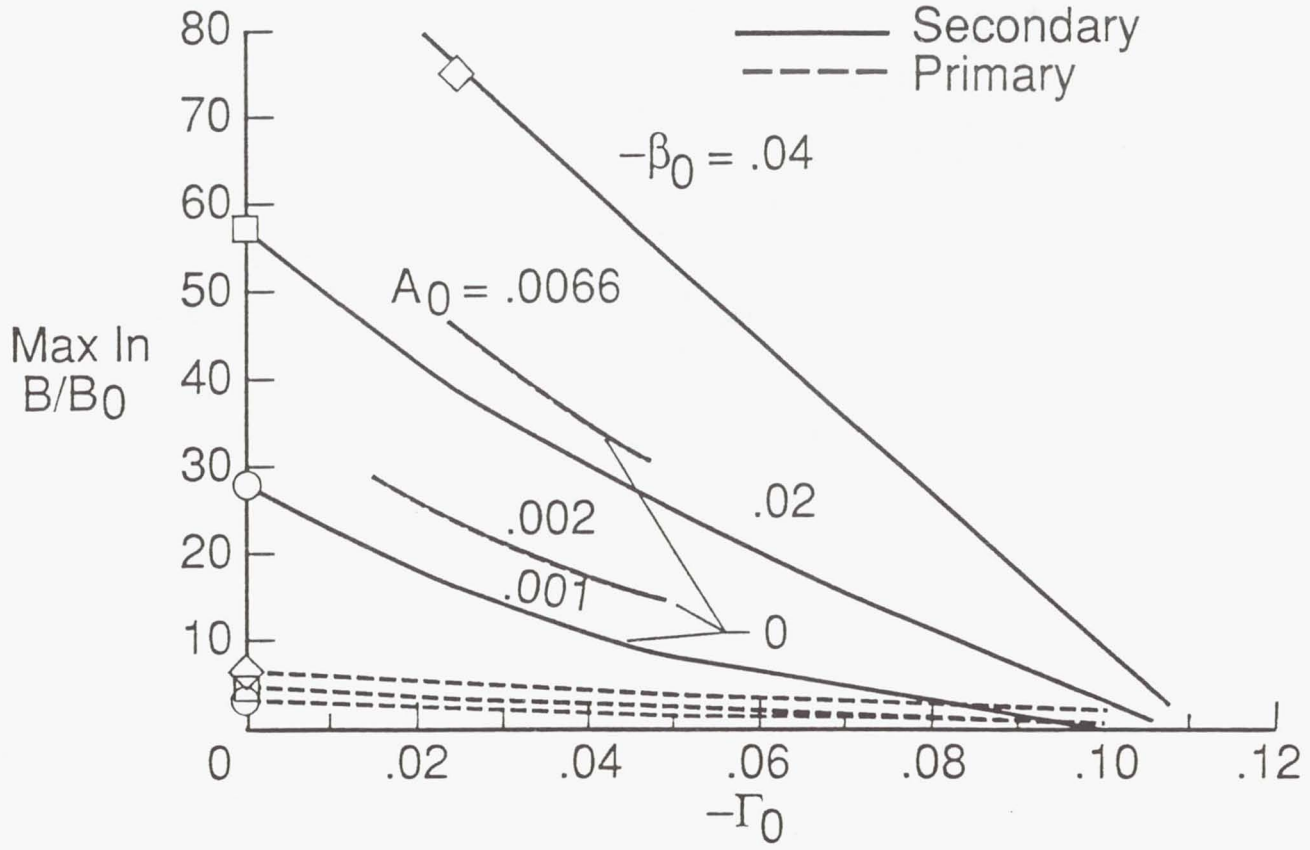


Fig. 7 Effect of suction parameter on the maximum amplification factors of both the primary wave and the secondary 3D subharmonic at various pressure gradient parameters, $A_0$=.001, $b$=.15, and $F$=60.

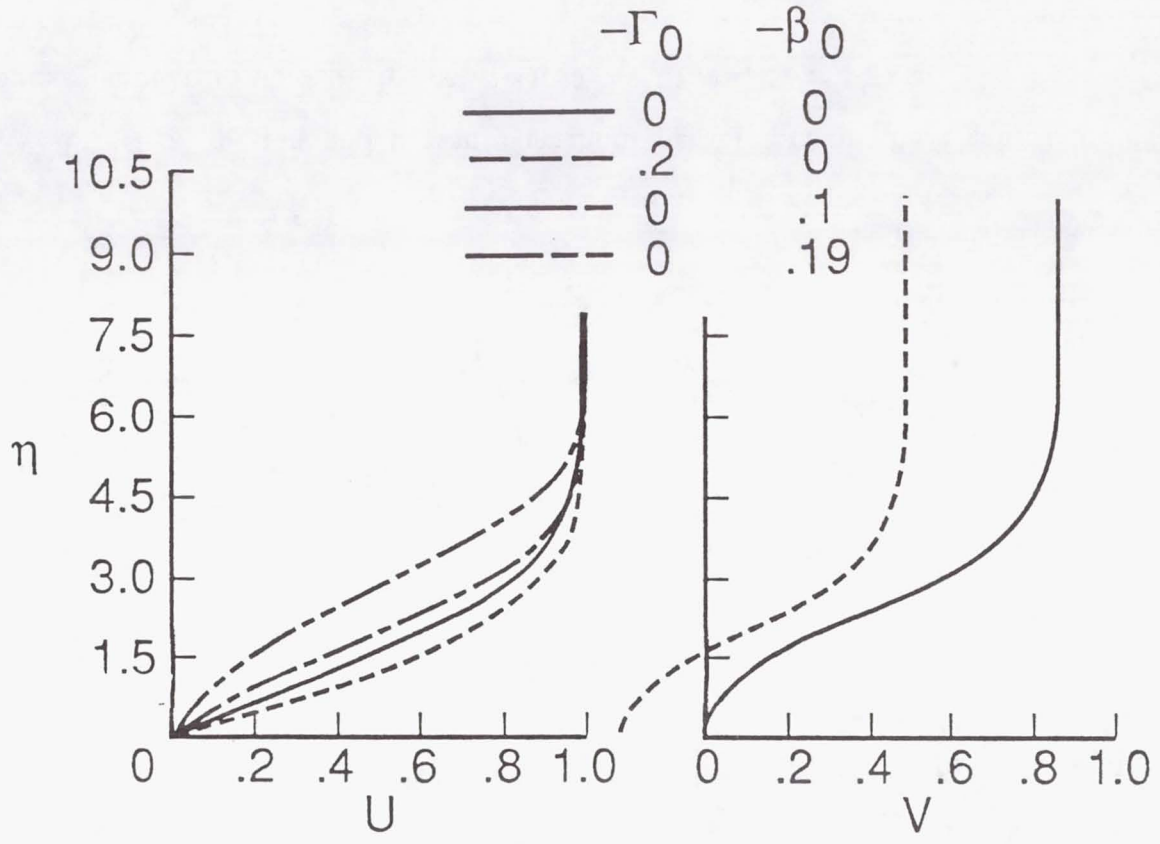


Fig. 8 Effect of suction and pressure gradient parameters on mean flow profiles.

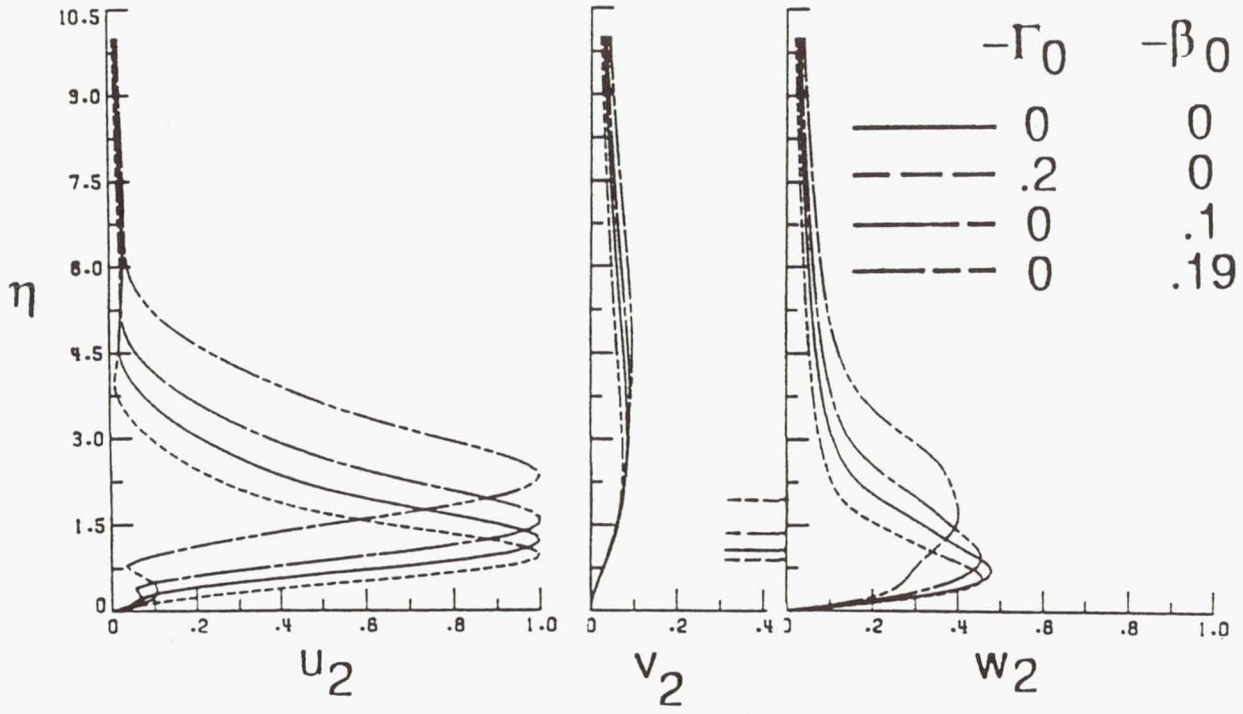


Fig. 9 Effect of suction and pressure gradient parameters on the eigenmodes of the secondary subharmonic disturbance, $R = 1050$, $A = .01$, $b = .15$, and $F = 60$.

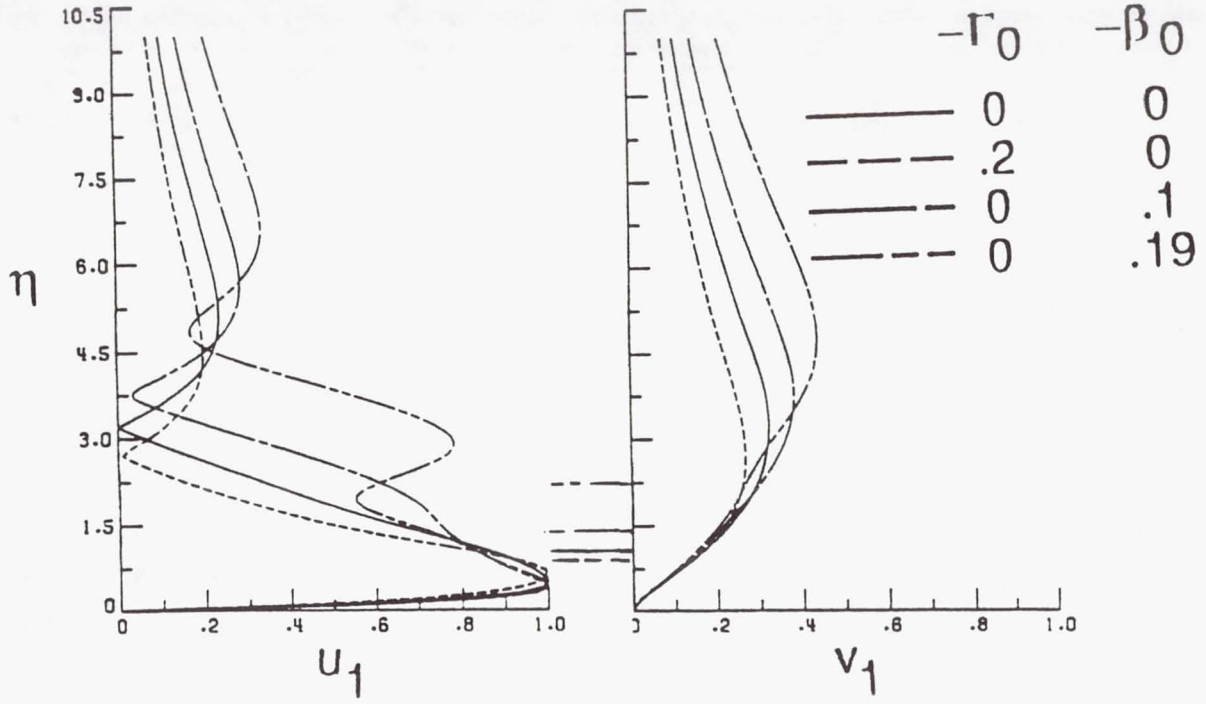


Fig. 10 Effect of suction and pressure gradient parameters on the eigenmodes of the primary wave, $R = 1050$ and $F = 60$.

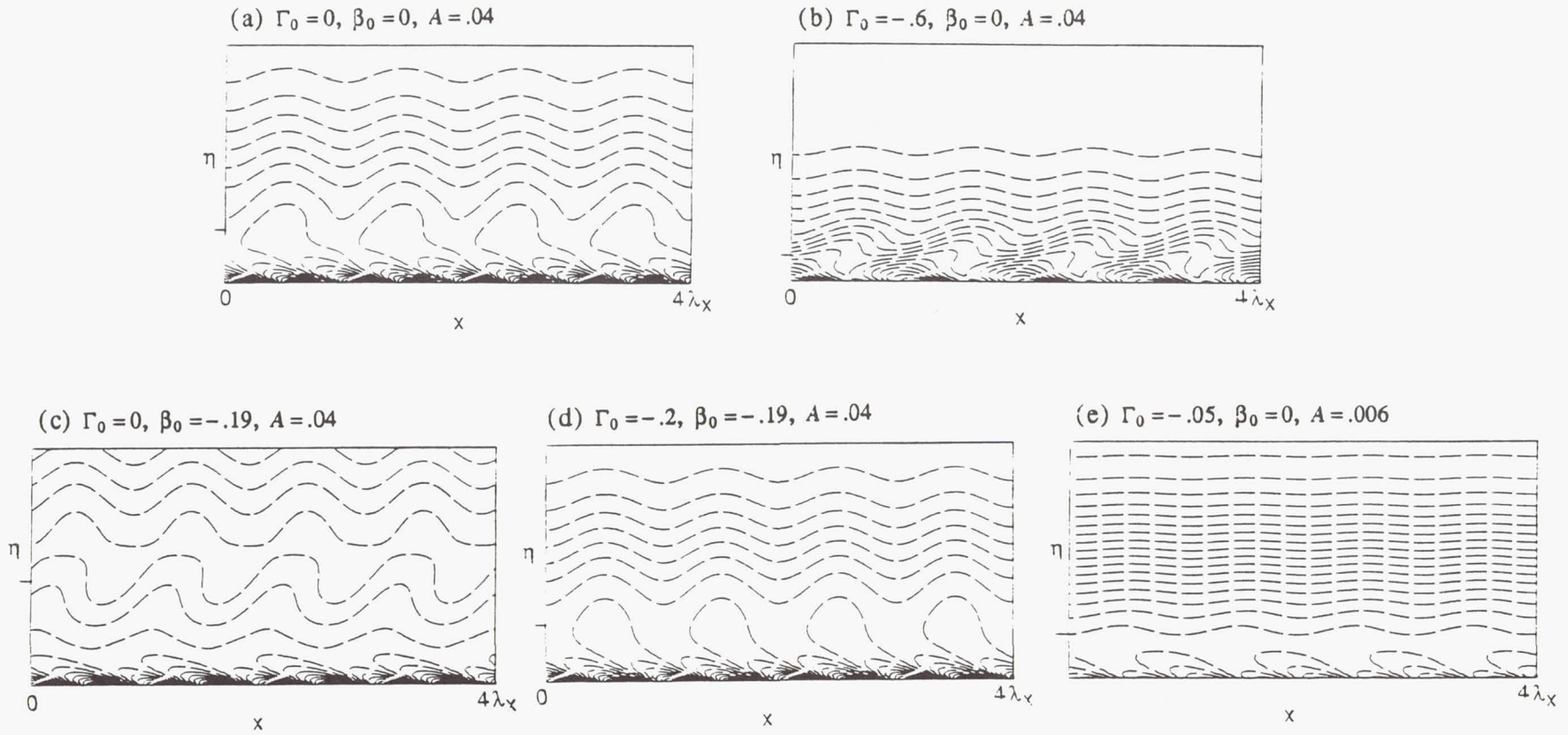


Fig. 11 Initial 2D vorticity contours of the basic flow at different suction and pressure gradient parameters. Flow direction is from left to right, $R = 1050, F = 60$.

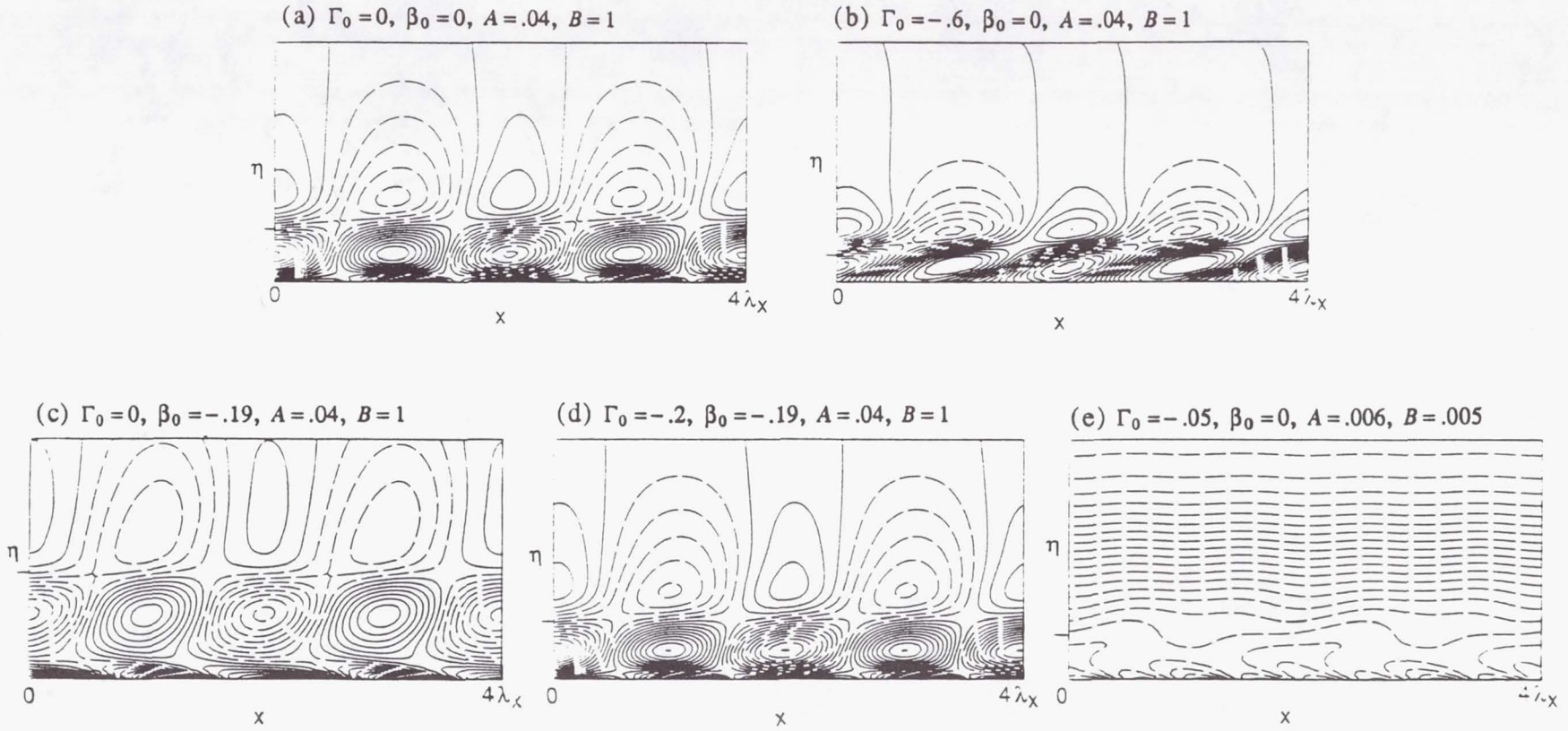


Fig. 12 Spanwise vorticity contours of the 3D flow in the $x-y$ plane at $z=0$ for different suction and pressure gradient parameters. $R$ = 1050, $b$=.15, and $F$=60.

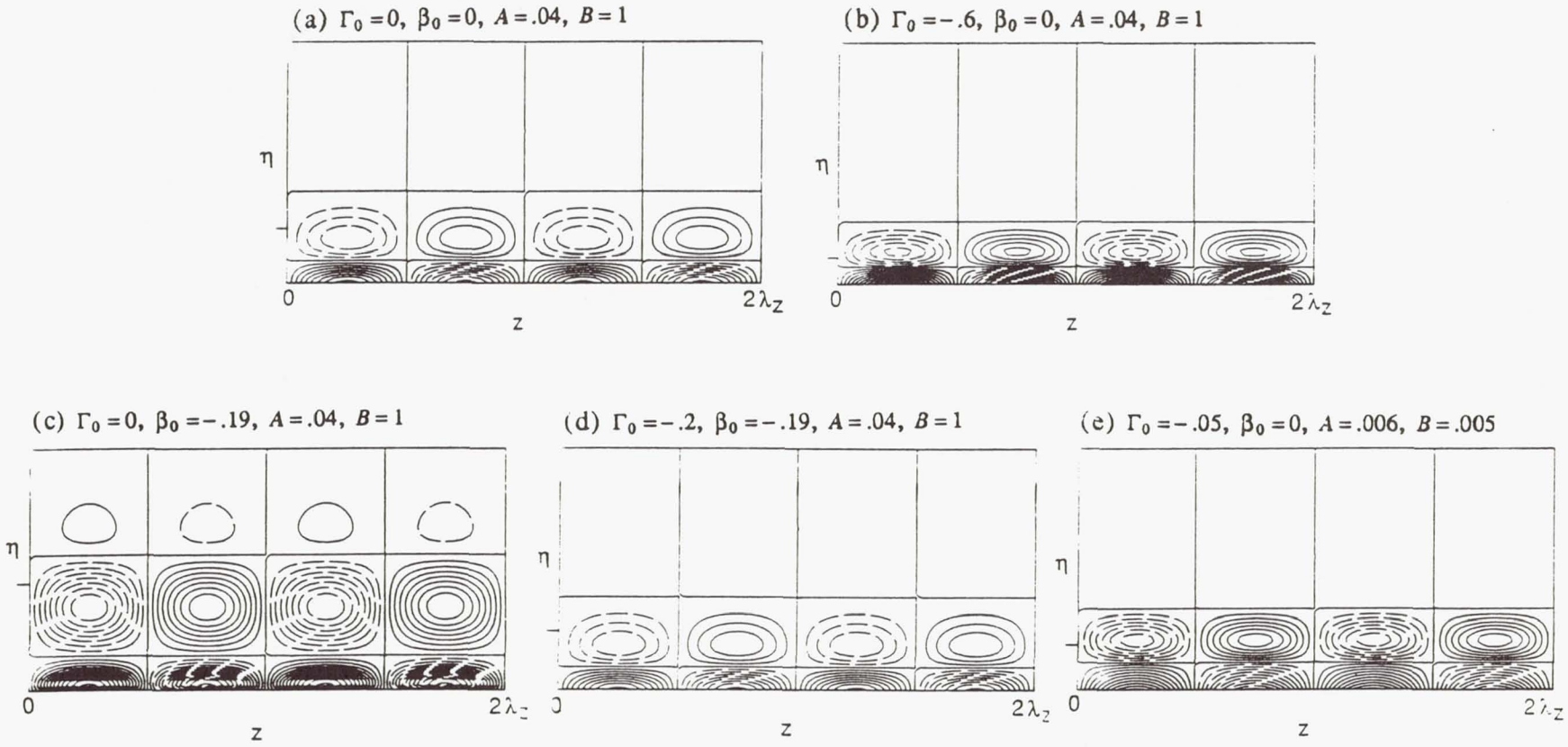


Fig. 13 Streamwise vorticity contours of the 3D flow in the $z-y$ plane at $x=0$ for different suction and pressure gradient parameters. $R = 1050$, $b = .15$, and $f = 60$.

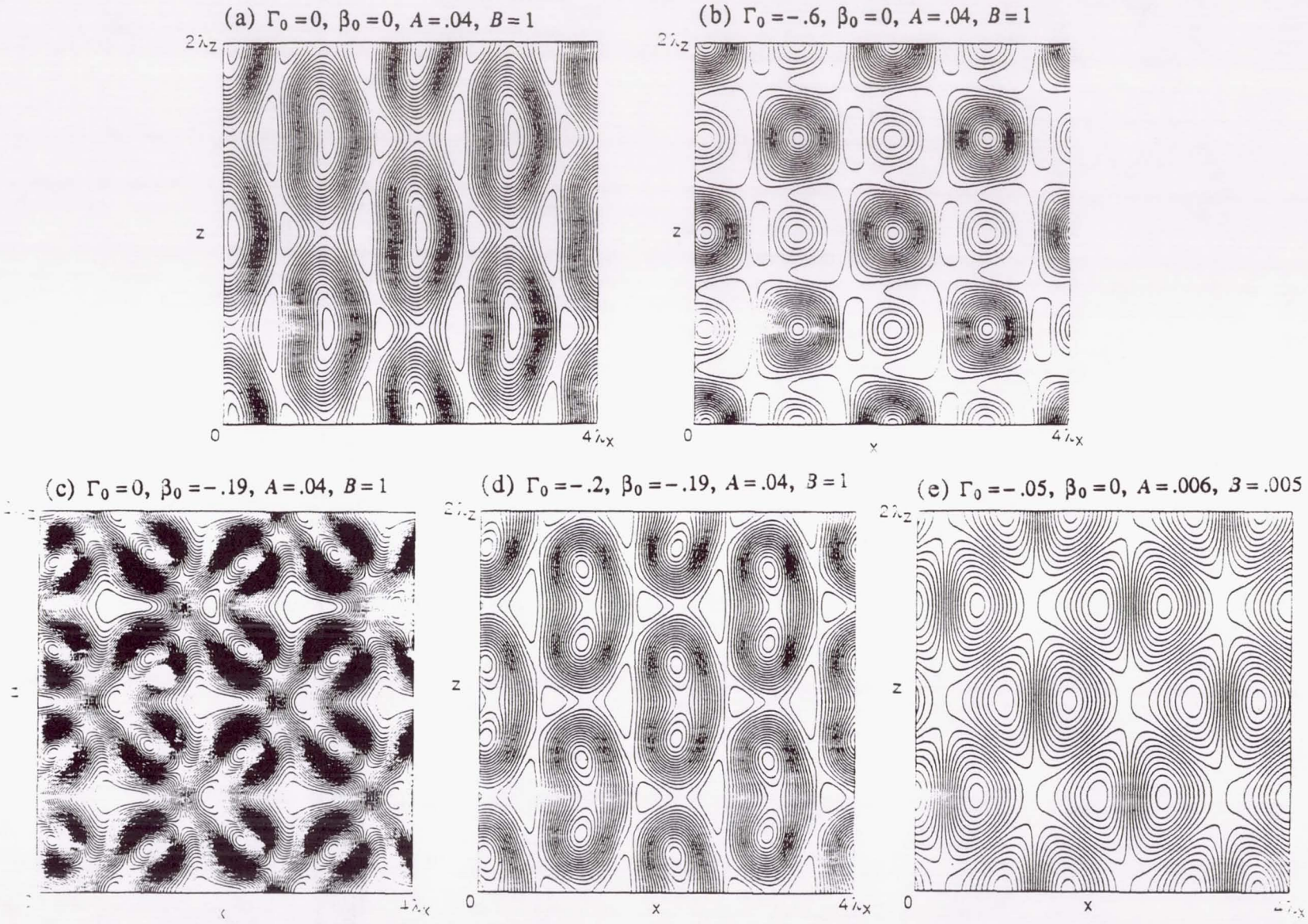


Fig. 14 Total vorticity contours of the 3D flow in the $x-z$ plane almost at the $y$-location of the critical layer for different suction and pressure gradient parameters. $R = 1050$, $b = .15$, and $F = 60$.

NASA
National Aeronautics and Space Administration

# Report Documentation Page

| 1. Report No. | 2. Government Accession No. | 3. Recipient's Catalog No. |
|---|---|---|
| NASA CR-4306 | | |

**4. Title and Subtitle**

Effect of Suction on Controlling the Secondary Instability of Boundary Layers

**5. Report Date**

July 1990

**6. Performing Organization Code**

**7. Author(s)**

Nabil M. El-Hady

**8. Performing Organization Report No.**

**10. Work Unit No.**

505-60-21-06

**9. Performing Organization Name and Address**

Analytical Services & Materials, Inc.
Hampton, VA 23666

**11. Contract or Grant No.**

NAS1-18599

**13. Type of Report and Period Covered**

Contractor Report

**12. Sponsoring Agency Name and Address**

National Aeronautics and Space Administration
Langley Research Center
Hampton, VA 23665-5225

**14. Sponsoring Agency Code**

**15. Supplementary Notes**

Langley Technical Monitor: Ajay Kumar
Final Report

**16. Abstract**

The effect of suction on controlling the three-dimensional secondary instability is investigated for a boundary layer with pressure gradient in the presence of small but finite amplitude Tollmien-Schlichting wave. The focus is on principal parametric resonance responsible for strong growth of subharmonics in low disturbance environment. Calculations are presented for the effect of suction on the onset and amplification of the secondary instability in Blasius and Falkner-Skan flows, as well as its effect on controlling the production of the vortical structure.

| 17. Key Words (Suggested by Author(s)) | 18. Distribution Statement |
|---|---|
| Boundary Layer<br>Secondary Instability<br>Suction Control | Unclassified-unlimited<br>Subject Category 34 |

| 19. Security Classif. (of this report) | 20. Security Classif. (of this page) | 21. No. of pages | 22. Price |
|---|---|---|---|
| unclassified | unclassified | 40 | A03 |

**NASA FORM 1626** OCT 86

For sale by the National Technical Information Service, Springfield, Virginia 22161-2171

NASA-Langley, 1990